Article

A fusion learning method for the age-related macular degeneration diagnosis based on multiple sources of ophthalmic digital images

Han Wang [1,2,3,4,*] and Junjie Zhou [2,4,5], Zhoujie Tang[3,4], Chengde Huang[3,4], Jie yang[6], Yi Pan[8,*] and Kelvin KL Chong [1,*]

1 The Faculty of Medicine, The Chinese University of Hong Kong, Hong Kong, China; 1155187855@link.cuhk.edu.hk; chongkamlung@cuhk.edu.hk
2 The faculty of Data Science, City University of Macau, Macau, China; D20092100037@cityu.mo
3 Beijing Institute of Technology, Zhuhai, China; luckanny111@163.com; 787704098@qq.com; 1479653329@qq.com
4 The department of AI and big data application, Zhuhai Institute of Advanced Technology Chinese Academy of Sciences, Zhuhai, China; wanghan@ziat.ac.cn
5 Hong Kong Baptist University, Hong Kong, China; D22092100275@cityu.mo
6 College of Artificial Intelligence, Chongqing Industry＆Trade Polytechnic, China 40800; jie.yang@connect.um.edu.mo
7 Biomedical Engineering，GuangDong Mediacl University，DongGuan，China；jason@ziat.ac.cn
8 Shenzhen Institute of Advanced Technology Chinese Academy of Sciences, Shenzhen China 518000; rt.xie@siat.ac.cn; yi.pan@siat.ac.cn
9 Hong Kong University of Science and Technology, Hong Kong, China; christinayq@gmail.com
10 Jinan University Affiliated Shenzhen Eye Hospital, China 51800; lina_h@126.com

* Correspondence: H.W. 1155187855@link.cuhk.edu.hk; Y.P. yi.pan@siat.ac.cn; K.K.C. chongkamlung@cuhk.edu.hk; L.H. lina_h@126.com.

Abstract: Age-related Macular Degeneration (AMD) is one of the most causes for elders' vision loss, early screening and treatment are the most efficient way to reduce the rate of blindness. AI-based methods based on ophthalmic images play a gat potential for AMD diagnosis. However, the difficulty of computing device obtaining, multiple evidence of image sources, time-wasting, and low level of explanation are challenges for AI models applicated in clinics. Thus, this study proposed a fusion learning method for AMD detection. Three steps are involved, which are image feature extraction, feature matrix fusion, and MLP-based AMD classification. Unsupervised (Hierarchical Clustering, SVM, and ResNet-K Means), supervised (VGG-16 and ResNet) methods and the proposed method are compared based on Optical Coherence Tomography (OCT), Fundus Autofluorescence (FAF), regular fundus photography (RCFP) and Ultra-Widefield Fundus (UWF), respectively and comprehensively. Findings show that the proposed method presents a high performance for integrated ophthalmic image diagnosis, it is timesaving (0.09s per image) with high precision (0.95), sensitivity (0.93), specificity (0.92) and AUC (0.94). Thus, this study concluded that the proposed method is a solution to AMD automatic quick detecting based on multiple data sources. A real-world UWF database is involved from Shenzhen Aier Hospital. Practical and theoretical contributions are delivered. A reference value for medical diagnosis based on multiple digital images is contributed.

Keywords: Age-related Macular Degeneration; Artificial Intelligence; Machine Learning; Optical Coherence Tomography; Fundus Autofluorescence; regular fundus photography; Ultra-Widefield Fundus

Preprints (www.preprints.org) | NOT PEER-REVIEWED | Posted: 21 November 2022 doi:10.20944/preprints202211.0392.v1

1. Introduction

Age-related Macular Degeneration (AMD) is an eye disease related to symmetric central chorioretinopathy, which is one of the most common ophthalmic causes of vision loss in the elder groups(1). Around 9.7% of the global loss of vision cases are related to AM(2). Causes involve ages, genes, habits, and environments. Diagnosis based on fundus images is the major solution for AMD detection(3,4). 7 types of methods include regular color fundus photography(RCFP)(1,4-6), Fundus Autofluorescence(FAF)(7), Infrared Imaging(IR)(8), Spectral-domain Optical Coherence Tomography(OCT)(9), Optical Coherence Tomography Angiography (OCT-A)(10), Scanning Laser Ophthalmoscopy(SLO)(11) and Ultra-Widefield Fundus (UWF) (12). 6 quantitative symptoms based on OCT are concluded as the macular epiretinal membrane (MEM)(13), retinal fluid accumulation(14), subretinal accumulation(15), subretinal hyperreflective material (SHRM)(16), vitreous warts (drusen)(17) and retinal detachment epithelium (18). When it comes to FAF, RCFP, and UWF, 13 potential symptoms may be able to be discovered, which are vitreous membrane in the macular region(19); 2) focal hyperpigmentation(20), MEM(13),choroidal neovascularization (CNV) in macular area (21,22), complete circular scotoma (completely black ring circle)(23), retinal pigment epithelial(RPE) detachment (24), subthreshold exudative choroidal neovascularization(25), sub-foveal intraretinal hemorrhage(26), large choroidal vessels and deep capillary plexus vessel in the macular region and glial scar tissue in the perimacular area(4,27), hemorrhagic spots and vitreous debris in the macular area(28), subretinal hemorrhage with residue in the perimacular region(1,4), glial scar in the macular region(29) and temporal margin hemorrhage residue in the macular region(1,4,30). However, it is time-consuming for ophthalmologists to detect AMD manually. AMD patients of the early stage are not easy to be detected because of the complexity of diagnosis based on fundus, the lack of ophthalmologists, and the shortage of fundus equipment, especially in developing areas.

Artificial Intelligence (AI) technologies has been widely applied to ophthalmology fields, deep learning (DL) and machine learning (ML) algorithms have been verified to be effective in the fundus disease early screening and prognosis(31,32). It presents advanced strengths and delivers opportunities for AMD detection with the limited resources. The algorithms of ophthalmic image classification and segmentations are increasingly to be focused during the recent years(33). However, issues of clinical data collection, ethical approval, fundus image algorithm optimization, labeled data enhancements, image key feature extractions, normalization and fusion of diagnostic images from multiple resources are still challenges for AI applied to ophthalmology theoretically and practically. Thus, solutions related to the challenges above are explored and deep collaborations of interdisciplinary scholars are performed in this study.

Thus, this study designed a fusion AI AMD diagnose system based on fusion deep learning models. Multiple algorithms are compared, where the cluster ML models of Hierarchical Clustering (HC)(34), ResNet-K Means(35) and Support Vector Machines (SVM)(36), the image classification models of VGG16(37) and ResNet50(38), and the proposed fusion AMD diagnosis system based on multi-layer perceptron (MLP)(39) network are involved. The structure of this paper is organized as the second section is related to the materials and methodologies, the third and fourth section is related to the results and discussions respectively, and the last chapter presents the conclusion and the future perspectives.

2. Materials and Methods

This study utilized four types of ophthalmic digital fundus images for AMD detections, which are OCT, FAF, RCFP, and UWF. Image cluster algorithms of HC, ResNet-K Means and SVM, classification algorithms of VGG16, ResNet50 and Unet and the

Preprints (www.preprints.org) | NOT PEER-REVIEWED | Posted: 21 November 2022 doi:10.20944/preprints202211.0392.v1

proposed fusion DL model are performed on the four types of datasets. And a data fusion mechanism is discussed at the end of the research.

2.1. Materials

The data resources of OCT, FAF and RCFP are from the open resources. The UWF is collected from Aier Hospital in China, which is an in-house dataset. OCT images are collected from Segmentation of Retinal OCT Images (optical coherence tomography) and Retinal OCT - C8 datasets on Kaggle website (https://www.kaggle.com/datasets/paultimothymooney/kermany2018(40) and https://www.kaggle.com/datasets/obulisainaren/retinal-oct-c8(41)), where 3000 and 29347 pictures of AMD and normal cases are included. The size of the OCT picture is (995±700)×(996±200). FAF photos are from Retinal Fundus Images dataset in Kaggle platform(https://www.kaggle.com/datasets/kssanjaynithish03/retinal-fundus-images)(42), 1947 AMD images and 2874 normal images are included. The size of the FAF picture is 512×512. Two open resources are related to RCFP, which are Retinal Disease Classification (https://www.kaggle.com/andrewmvd/retinal-disease-classification) (43) and Ocular Disease Recognition (https://www.kaggle.com/andrewmvd/ocular-disease-recognition-odir5k)(44), where 445 AMD and 2874 normal images are included. The size of the RCFP picture is (2000 ± 1500) × (2000 ± 1000). 2300UWFimages are collected from Shenzhen Aier hospital, which are obtained by using the Optos device, the size of the UWF figure is 2600×2048. 1100 and 1200 images are related to AMD and normal subjects. Ethic approval documents have been obtained from the ethic group in Shenzhen Aier hospital (Approval number: IRB-SOP-016(F)-002-03). The "data access authorization & medical data ethics supporting document" from Shenzhen Aier Eye Hospital (both Chinese and English versions) of this study is available online at https://github.com/luckanny111/macular_fovea_detection.

2.2. Methods

A data preprocessing is performed on datasets of OCT, FAF, RCFP and UWF respectively. Tools of Pyhon 3.8.3, Pytorch 1.8.1, Cuda 11.1 and double GPU version of 3060Ti are utilized in this study. Three kinds of AMD diagnosis methods are explored in this research, which are (1) unsupervised learning methods of HC, ResNet-K Means and SVM, (2) supervised learning methods of VGG16 and ResNet16, (3) proposed multiple data sources fusion method based on MLP model and image feature extraction models.

2.2.1 Data preprocessing

2.2.1. Data preprocessing on OCT dataset

There are 3000 (AMD) and 29347 (normal) figures are included in the original dataset. The figure 1 is the example of OCT original figures, where A, B and C are related to AMD cases, D, E and F belongs to normal clusters. The symptom of drusen is presented in AMD images. A picture enhancement process is performed on the AMD pictures, which includes image rotating, data generation based on Conditional Generative Adversarial Network (CGAN)(45), and noise reduction. GGAN is an effective way for data enhancement, especially for medical image generations(45). CGAN was proposed by Mirza and Osindero in 2014 (46). Comparing to the normal Gan, the generator exhibits higher efficiency with extra information of classification labels y. As the following formula shown, the objective function of mini-max game between the generator and discriminator is the key for CGAN performing(46).A salt and pepper noise (SPN) filtering is performed on the generated figures(47). At the end, the size of OCT images is resized as 512×512. Correlation based Feature Selection (CFS) algorithm is performed on the preprocessed OCT database to generate the segmented OCT database.

$$min_G\, max_D\, V\,(D,G) = E_{x\sim pdata(x)}[log\, D(x|y)] + E_{z\sim P_z(Z)}[log(1 - D(G(z|y)))]. \quad (1)$$

Preprints (www.preprints.org) | NOT PEER-REVIEWED | Posted: 21 November 2022 doi:10.20944/preprints202211.0392.v1

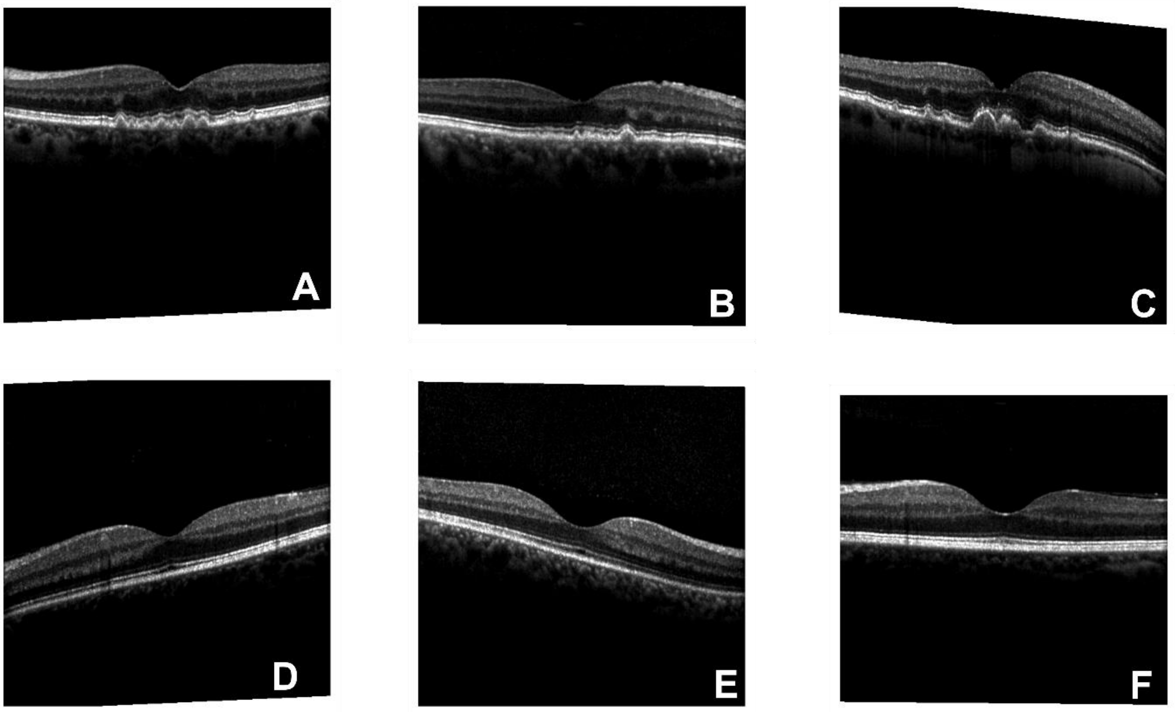

Figure 1. Original figures of OCT images

2.2.2. Data preprocessing on FAF dataset

There are 1947 AMD and 2874 normal images in FAF dataset. Examples of AMD (A, B and C) and normal (D, E and F) are illustrated in Figure 2. Drusen and CNV are emerged in AMD images. The symptom of CNV is hard to be noticed in OCT, RCFP and UWF, especially when it comes to RPE abnormalities in the late stage of AMD. However, the contrast medium of fluorescence may cause the eye allergic action, which is a potential threat for patients(48). A binary processing is performed on the FAF dataset. A rotating is performed on the dataset.

Preprints (www.preprints.org) | NOT PEER-REVIEWED | Posted: 21 November 2022 doi:10.20944/preprints202211.0392.v1

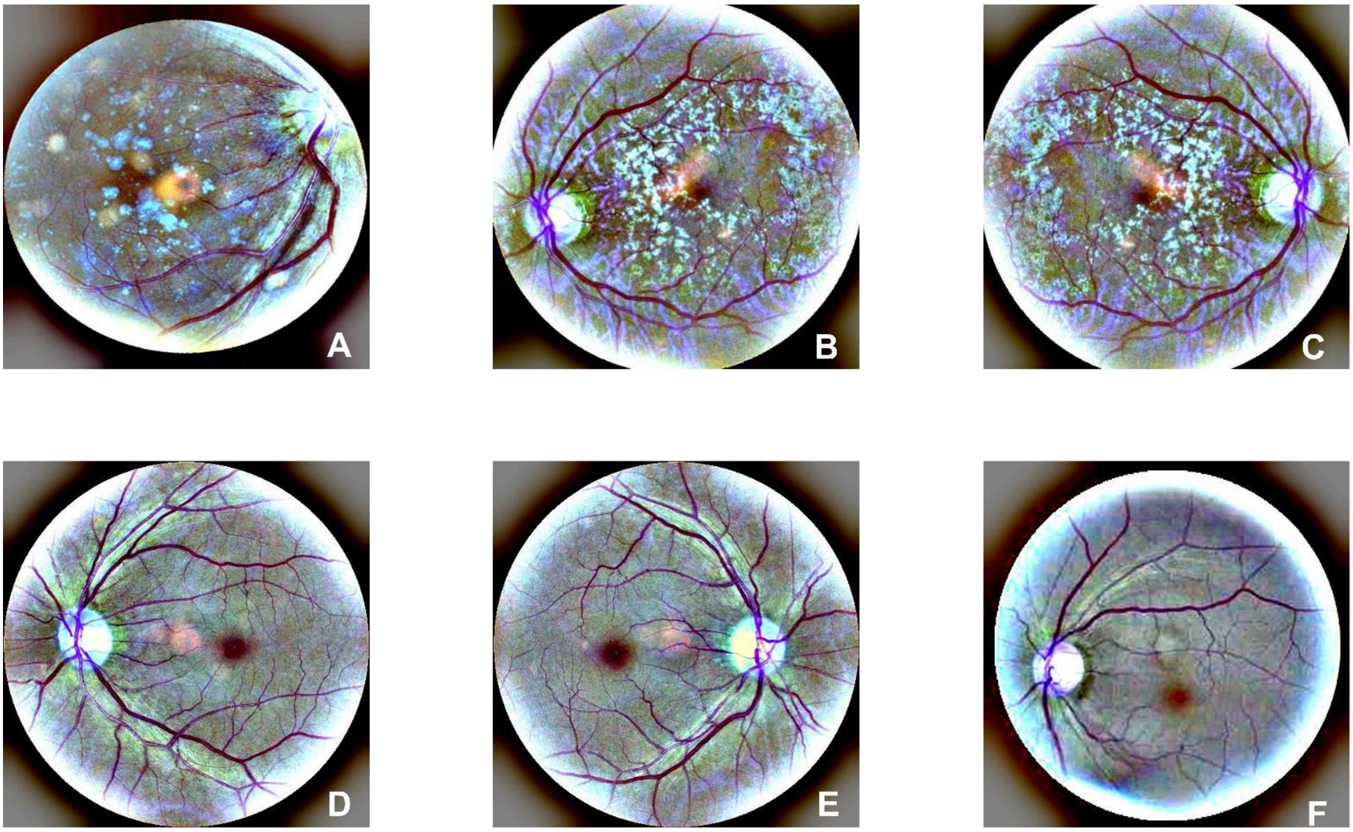

Figure 2 Original figures of FAF images

2.2.3. Data preprocessing on RCFP dataset

445 AMD and 2874 normal RCFP original images are collected from open sources. Examples of AMD (A, B and C) and normal (D, E and F) are illustrated in Figure 3. The drusen is clearly illustrated in A and B, and symptoms of hemorrhagic spots, vitreous debris and subretinal hemorrhage with residue the perimacular region are presented in A. The subfigure of C shows symptoms of large choroidal vessels and deep capillary plexus vessel in the macular region and glial scar tissue in the perimacular area. Preprocessing of rotating and SPN adding noise are performed on the AMD RCFP images.

 doi:10.20944/preprints202211.0392.v1

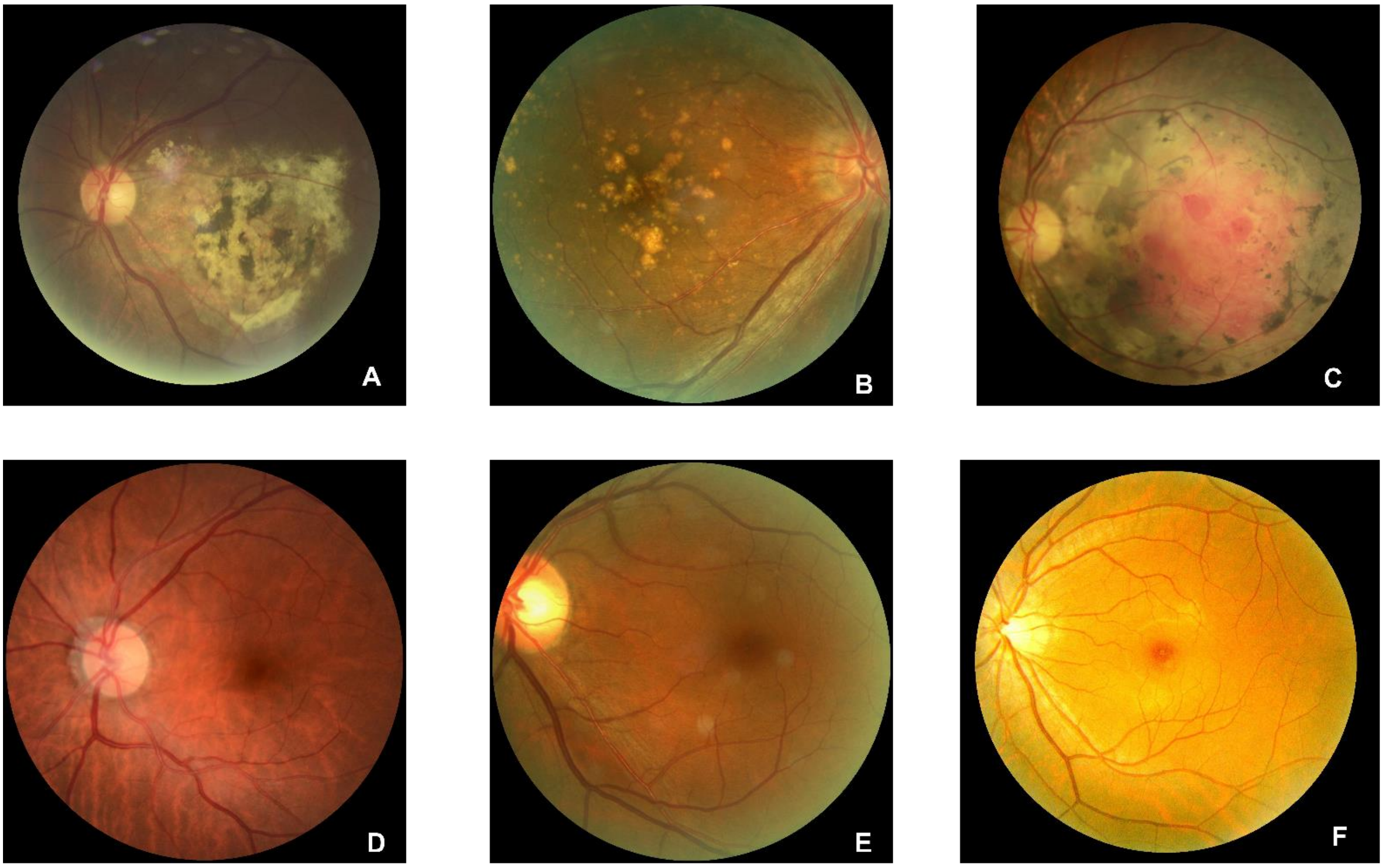

Figure 3 Original figures of RCFP images

2.2.4. Data preprocessing on UWF dataset

1100 AMD and 1200 normal original figures of UWF are collected. Examples of AMD (A, B and C) and normal (D, E and F) are illustrated in Figure 4. The drusen is in the macular area in A and B. The symptom of CNV is illustrated in A and C. The subfigure of C also presents a lesion of sub-foveal intraretinal hemorrhage. Since the size of original UWF is very large. The key feature is easy to be ignored by the models, leading to a low accuracy. Besides, a high level for computing and room saving resources are requested. To higher the precision and save the time and resource of deep learning models training process, this study extracted the Region of Interests (ROI) of UWF for AMD classification tasks. This ROI is defined as the area with the fovea as the center and the distance from the center of the optic disk (OD) to the fovea as the radius(33). The fovea and OD center have been located in authors former research(33). Preprocessing of rotating and additive noise performance based on SNP roles are parsed on the AMD UWF images.

Preprints (www.preprints.org) | NOT PEER-REVIEWED | Posted: 21 November 2022 doi:10.20944/preprints202211.0392.v1

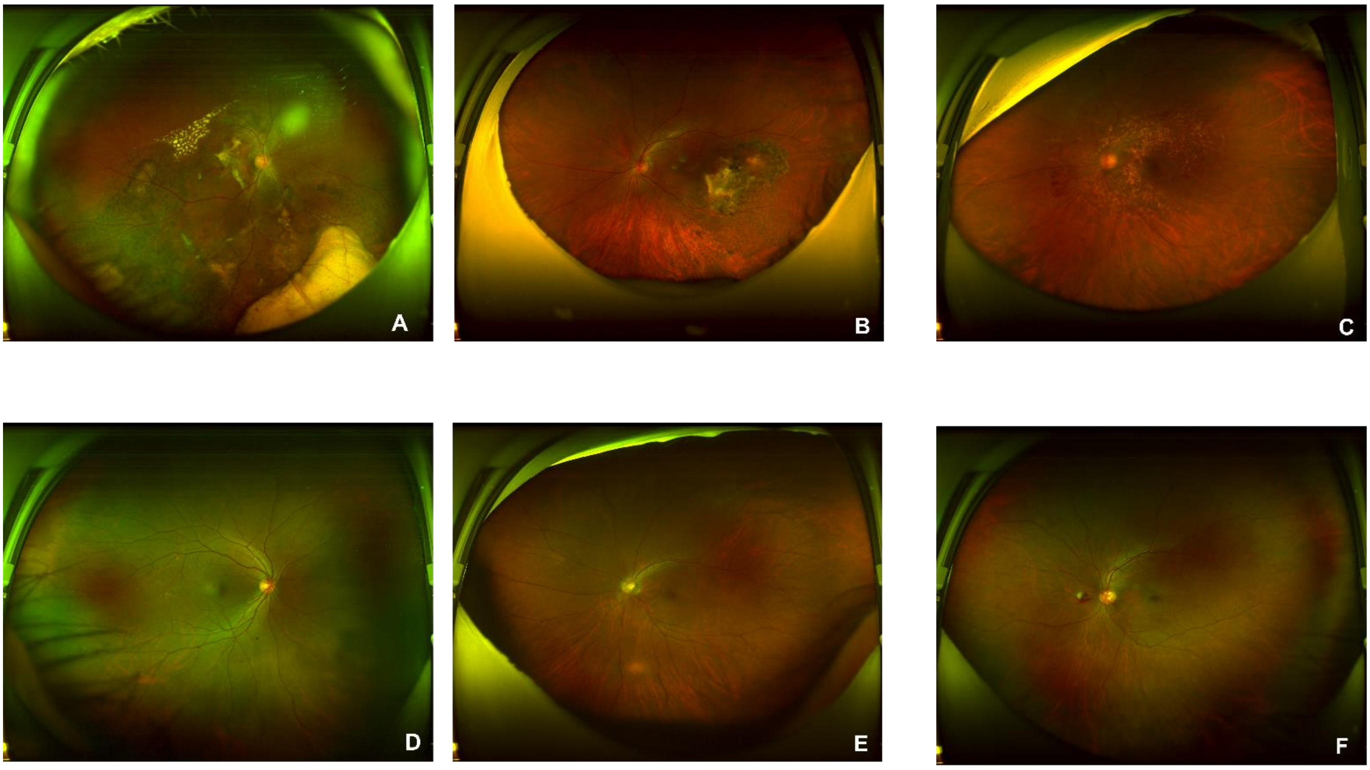

Figure 4 Original figures of UWF images

2.3 AMD detection methods

2.3.1 Unsupervised learning methods

This study utilized two unsupervised ML methods of Hierarchical Clustering and Support Vector Machines, which are significant algorithms for image clustering. The advantages of unsupervised learning methods are timesaving and resource saving. The data-driven algorithm could be a good choice for feature extraction. However, it is unexplainable and unable to control when it comes to medical diagnosis. It may not be able to cluster into specific required classes. A low level of trust and efficiency are exhibited. This study randomly selects (100, 150 and 200) AMD images and (100, 150 and 200) normal images, utilizes HC, ResNet-K Means (ResNet is for feature extraction, K-means for clustering) and SVM to cluster images into two classes, and identifies the highest accuracy of this method for AMD detection. These three algorithms are also utilized for feature extraction by clustering figures into the most optimal number of categories. Parameters of the most optimal number of clustering algorithms are decided by within-cluster sum of squared errors (SSE). The parameter of HC is identified as the following (0.645*tree. distance). Parameters of ResNet-K Means are identified as the following (Resize 224*224, n_clusters=2). Parameters of SVM are identified as the following (gray, orientations=12, block_norm='L1', pixels_per_cell=[8, 8], cells_per_block=[4, 4], visualize=False, transform_sqrt=True).

2.3.2 Supervised learning methods

The supervised learning methods of VGG16 and ResNet are applied in AMD classification. Comparing to the unsupervised ML methods, advantages of classification algorithms are a relatively high accuracy. However, it is time consuming with a high resource requirement. When it comes to medical diagnosis, there are 13 convolutional layers, 3 fully connected layers and 5 pool layers in the VGG16 model (Figure 5). The architecture of Resnet is the same as VGG16, the difference from VGG16 is that Resnet adds skip layers between convolution layers.

 doi:10.20944/preprints202211.0392.v1

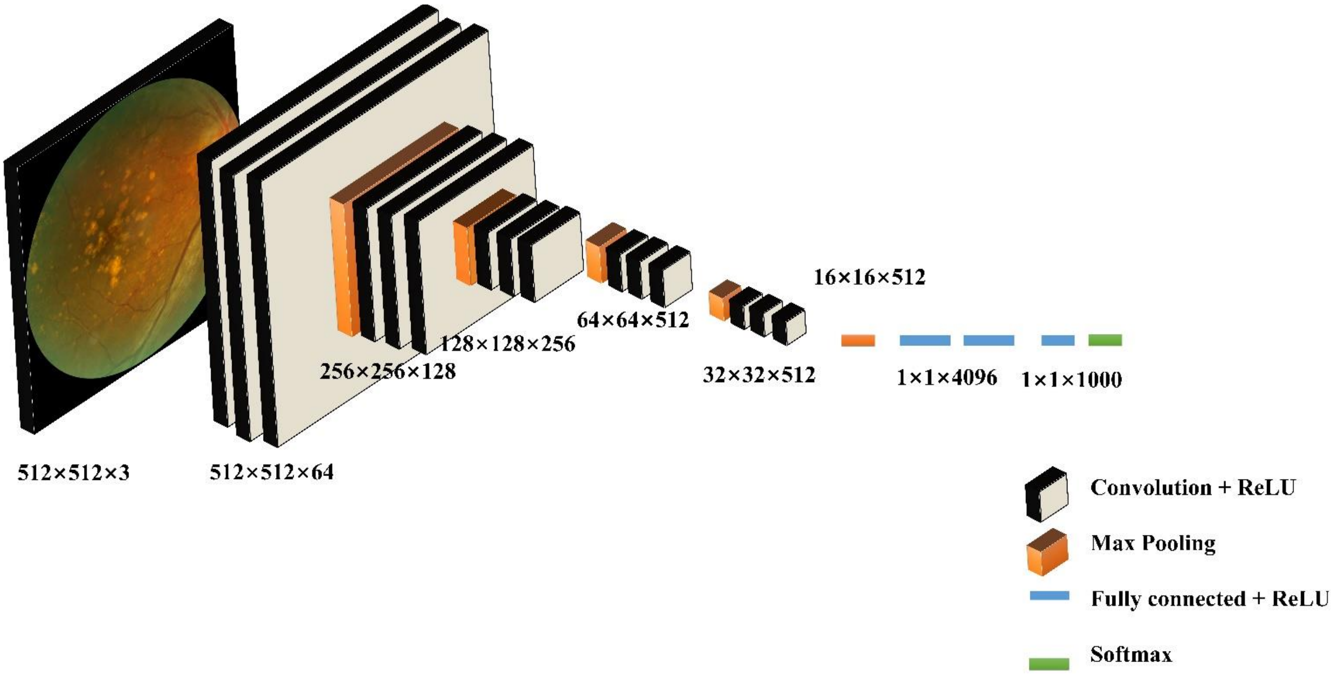

Figure 5 The structure of VGG16 for AMD detection

2.3.3 MLP-based fusion method for multiple data sources

There are three steps of the proposed method, which are feature extraction, feature fusion and AMD classification.

1. Following features are involved in to the first step. (1) One-hot labels by image types of OCT, segmented OCT, FAF, RCFP and UWF. (2) Texture features of image contrast, dissimilarity, homogeneity, energy, correlation and angular second moment (ASM); (3) cluster labels by HC, ResNet-K Means and SVM cluster algorithms, (4) image features extracted by ResNet. Texture features are extracted by scikits-image function in Python program language. The number of clusters for ResNet-K Means and HC model is decided by the measurement indicator of SSE.
2. Feature fusion.

   As the figure 6 shown, features matrix is established by adding "0" in the missing location. Three dimensions of texture features (the first line), cluster labels (the second line) and extracted features from the ResNet last layer (the last line) are combined in the matrix. The output feature matrix is 1×1×2048.
3. AMD classification.

   As the figure 6 shown, the combined feature matrix is input into the MLP network and predict into two classes, which are AMD (labeled as 1) and normal (labeled as 0).

 doi:10.20944/preprints202211.0392.v1

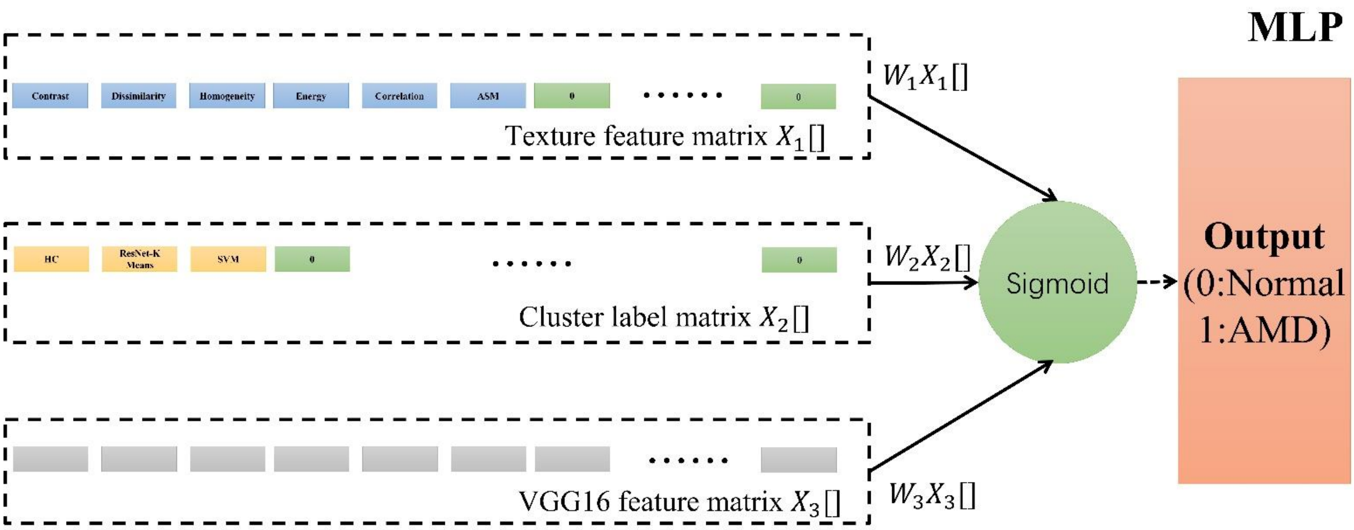

Figure 6 The architecture of feature fusion and MLP classification

3. Results

3.1. Data preprocessing results

After a data preprocessing process, 44347(15000 AMD and 29347 normal) OCT figures, 64143 (5841 AMD and 8622 normal) FAF images, 4654 (1780 AMD and 2874 normal) RCFP figures and 14463(5841 AMD and 8622 normal) UWF photos are output. The process and data enhancement examples are illustrated in the Figure 7.

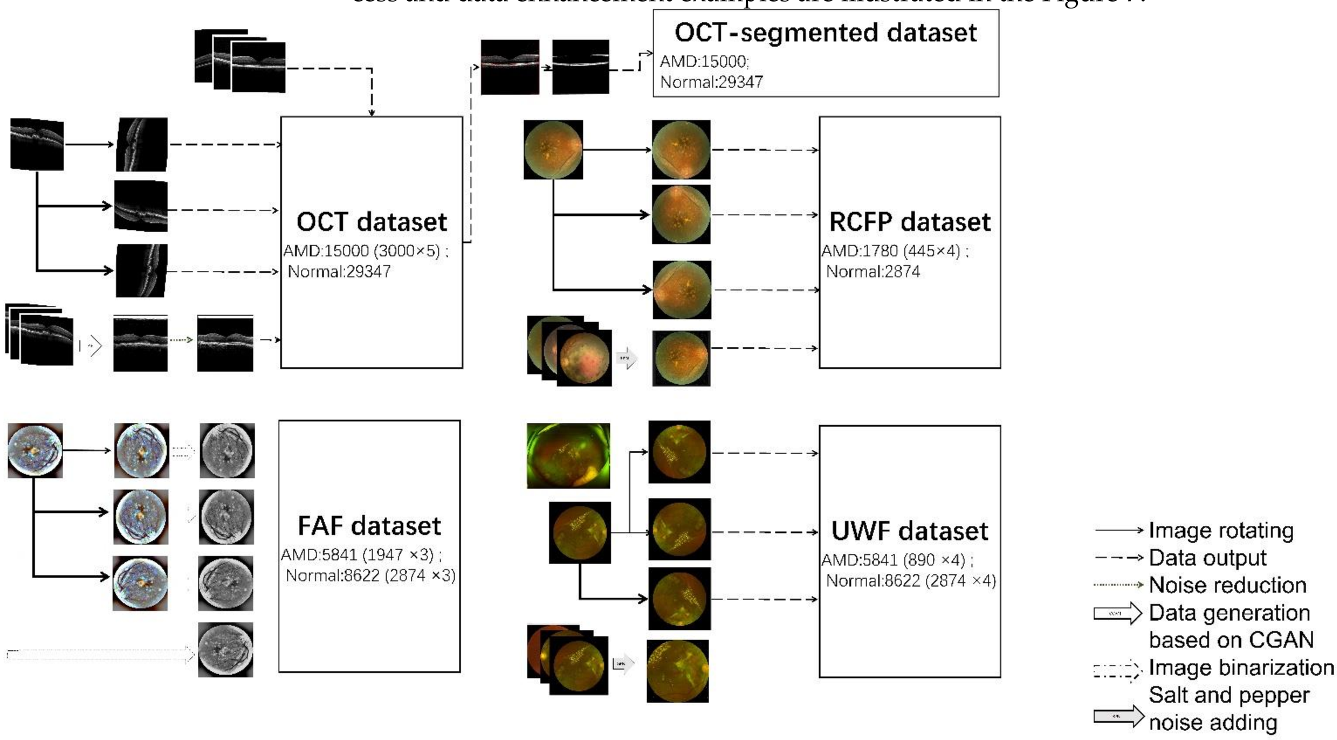

Figure 7 data preprocessing process on OCT, FAF, RCFP and UWF

The parameters of CGAN models on OCT images are set as the following, batch size is set as 32, number of channels is set as 3, size of latent vector is set as 100 epochs are set as 300, generator loss rate is set as 0.05, discriminator loss rate is set as 0.0025, Adam Optimizers beta1 is set as 0.5. The sizes of input and output image are same as 256 × 256. 3000

Preprints (www.preprints.org) | NOT PEER-REVIEWED | Posted: 21 November 2022 doi:10.20944/preprints202211.0392.v1

AMD images are input as the training dataset. A cross validation is performed on the training model. The loss value of generator and discriminator is 0.1122 and 0.0352 respectively. 11454.39294 seconds are utilized for this model training and 0.0186 second is used for generating one new image. The example of generating pictures of 1 batch, 60 batch, 120 batch, 180 batch, 240 batch, 300 batch and the SNP removal processed image are shown in the Figure 8.

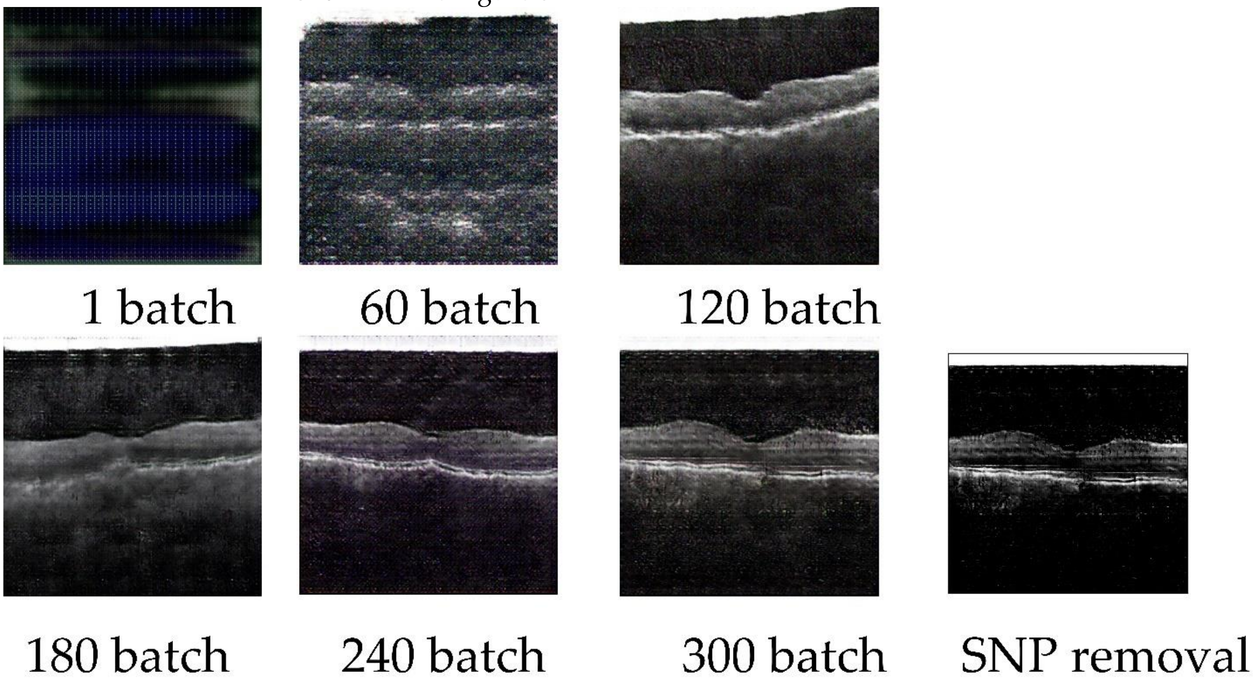

Figure 8 CGAN OCT image generation workflow and preprocess based on SNP

Figures in the OCT database are processed by CFS algorithm to extract key features, which are output as OCT-segmented database (Figure 9). CFS model has been applied in to multiple medical image processes(49,50). As the Figure 9 shown, subfigure A is the original figure, B is related to image feature identification, C is the segmented OCT image. Shape features of the macular epiretinal membrane and choroid are extracted (white part shown in C).

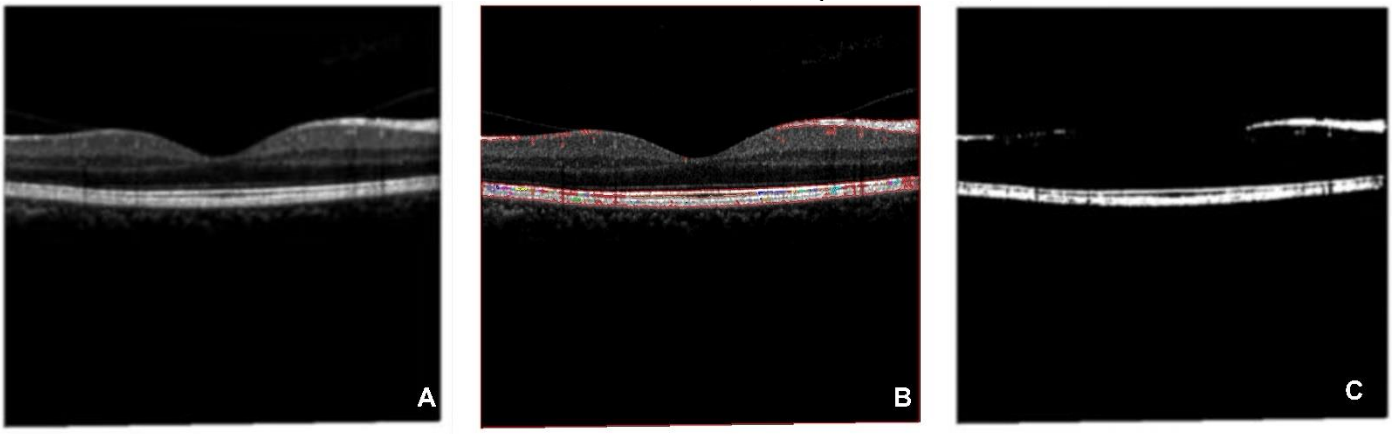

Figure 9 CFS process on OCT database (A is the original figure, B is related to image feature identification, C is the segmented OCT image).

The example of ROI extraction of UWF is presented in Figure 10. The left is original UWF figure, and the right is related to the ROI extracted image.

 doi:10.20944/preprints202211.0392.v1

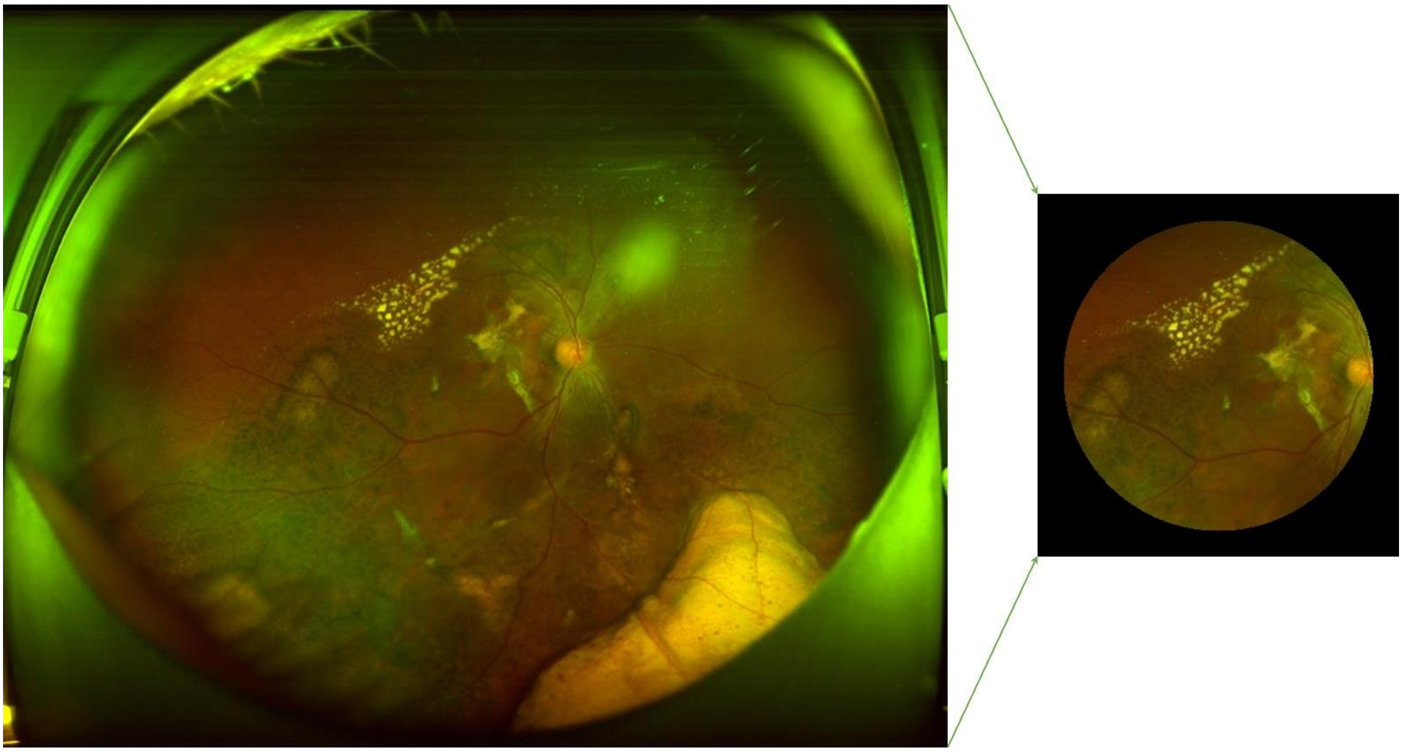

Figure 10 ROI extraction

The original image of RCFP(A), generated RCFP based on SPN (B), original image of ROI of AMD and normal UWF (C and E), generated ROI of AMD and normal UWF based on SPN (D and F) are illustrated in the Figure 11.

 doi:10.20944/preprints202211.0392.v1

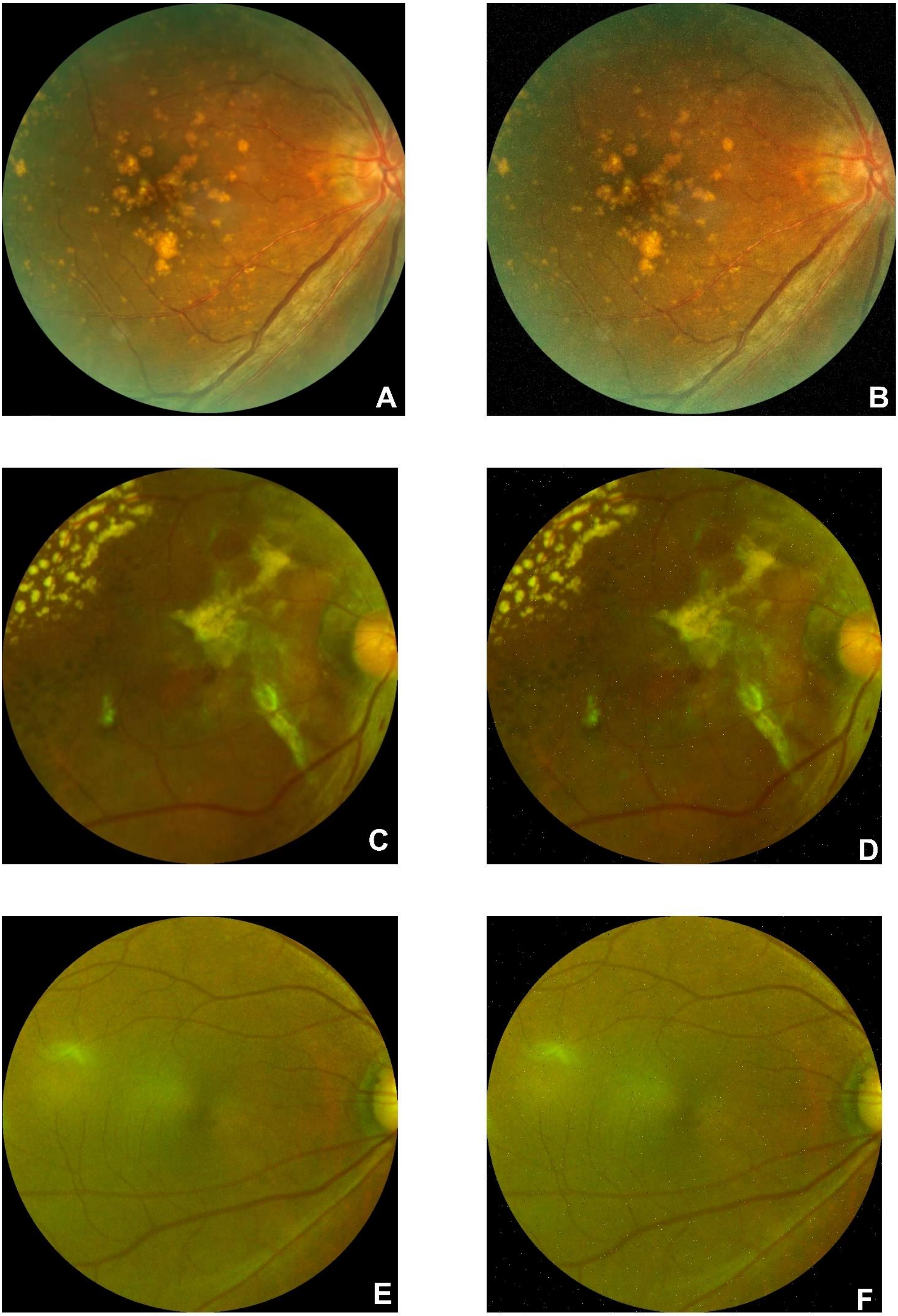

 doi:10.20944/preprints202211.0392.v1

Figure 11 Data enhancement based on SPN on RCFP (A and B) and ROI of UWF (C, D, E, and F)

3.2. MLP-based fusion method for multiple data sources

There are three parts for the proposed MLP-based fusion method. As for the first part of feature extraction. The feature of cluster label is decided by unsupervised learning methods, where parameters of the number of clustering for SVM is 2, which for HC and ResNet-K mean are decided by the inflection point for SSE-Cluster plotted figure. As the Figure 12 shown, the category results of HC for OCT, segmented OCT, FAF, RCFP and ROI of UWF are 5,4,4,7 and 8, which are 6,9,4,8 and 8 for the ResNet-K mean algorithm. There is no inflection point for original UWF figures, which is verified the conclusion that a ROI extraction based on UWF for AMD identification is necessary.

The Appendix A is an example of feature fusion, the dimension of normalized fused feature matrix for one picture is 15×2048. Image types of OCT, segmented OCT, FAF, RCFP and UWF, texture features of image contrast, dissimilarity, homogeneity, energy, correlation and ASM and cluster labels of HC, ResNet-K Means and SVM algorithms and image features extracted by ResNet are involved.

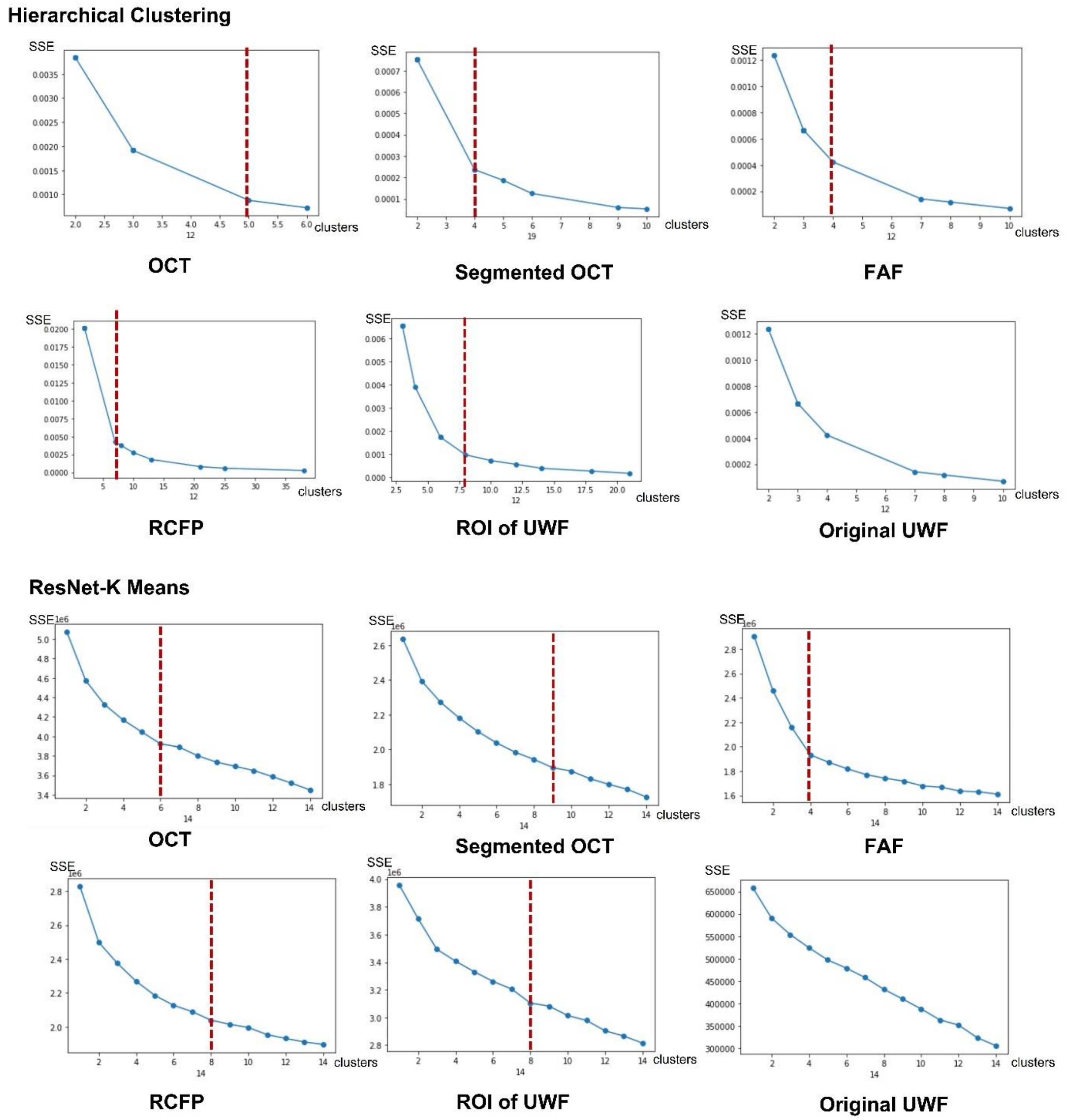

Figure 12 Relationship between SSE and clusters for HC and ResNet-K Means

3.3. *AMD detection results*

Results of AMD detection are presented in the Table 1. Indicators of accuracy, sensitivity, specificity, AUC and test time (per image) are algorithm measurement. Databases of OCT, segmented OCT, FAF, RCFP and UWF are tested on unsupervised and supervised learning methods respectively. Proposed MLP-based fusion method for multiple data sources is performed and comparing to other methods. Datasets of unsupervised are decided by random selecting 400 images from the database, where 50% are related to AMD. Datasets of supervised learning methods are segmented by 3:1 for training and verifying. 400 images (AMD occupies 50%) are selected for testing respectively.

There is no result output of HC model for RCFP and UWF when the cluster number set as 2. Average results values of accuracy, sensitivity, specificity, AUC and test time for all data types based on HC, SVM and ResNet-K Means are 53.57%, 56.02%, 89%, 0.5467 and 0.0133, 72.10%, 80.00%, 80.20%, 0.8667 and 0.099, and 59.26%, 58.49%, 48.58%, 0.73986 and 0.119.

Preprints (www.preprints.org) | NOT PEER-REVIEWED | Posted: 21 November 2022 doi:10.20944/preprints202211.0392.v1

Average results values of accuracy, sensitivity, specificity, AUC and test time for all data types based on VGG16 and Res-Net are 0.81964, 0.80752, 0.83122, 0.88804 and 0.127, and 0.59262, 0.58488, 0.48584, 0.73986 and 0.11882.

Average results values of accuracy, sensitivity, specificity, AUC and test time for all data types based on the unsupervised and supervised learning models and proposed method are 63%, 66%, 64%, 0.69 and 0.11, 80%, 77%, 0.77, 0.84 and 0.14, and 95%, 93%, 0.92, 0.94 and 0.09.

Results of accuracy, sensitivity, specificity, AUC and test time for proposed MLP-based method based on integrated databases are 94.06%, 94.22%, 93.26%, 0.9607 and 0.074, and 99%, 98.41%, 96.33%, 0.9823 and 0.065, and 90.11%, 87.06%, 88.98%, 0.9401 and 0.096, and 93.76%, 93.76%, 93.77%, 0.8924 and 0.121, and 98.12%, 97.06%, 95.47%, 0.9908 and 0.087, and 97.4%, 90.1%, 86.24%, 0.884 and 0.0886.

The proposed method shows the highest accuracy and relatively low consuming time for AMD detection based on OCT, segmented OCT, FAF, RCFP, UWF and integrated database. Unsupervised models are fastest model in tasks. Comparing the supervised and unsupervised methods, supervised models present an advantage for accuracy, sensitivity, specificity and AUC. Becides, AMD detection based on segmented OCT dataset presents the highest accuracy compared to other data sources.

Table 1 Average results values of accuracy, sensitivity, specificity, AUC and test time for all data types based on AMD detection models

Methods		**Training Dataset Test Dataset**	**Accuracy**	**Sensitivity**	**Specificity**	**AUC**	**Test time/second (Per image)**
Unsupervised learning methods	HC	OCT	53%	57.14%	82.0%	0.52	0.0138
		Segmented OCT	54.72%	52.60%	100%	1	0.0110
		FAF	53.%	58.33%	85%	0.12	0.0152
		RCFP	/	/	/	/	/
		UWF	/	/	/	/	/
		Average values for all data types	53.57%	56.02%	89%	0.5467	0.0133
	SVM	OCT	70%	70%	70%	0.79	0.115
		Segmented OCT	95.52%	93%	98%	0.9814	0.084
		FAF	94%	99%	89%	0.8911	0.112
		RCFP	53.5%	53%	54%	0.7562	0.117
		UWF	47.5%	85%	10%	0.235	0.067
		Average values for all data types	72.10%	80.00%	80.20%	0.8667	0.099
	ResNet-K Means	OCT	52.5%	51.49%	36.08%	0.6709	0.188
		Segmented OCT	93.53%	97.03%	81.82%	0.7939	0.174
		FAF	44%	12.5%	30.50%	0.9131	0.198
		RCFP	54.78%	53.42%	41.33%	0.6866	0.197
		UWF	51.5%	78.0%	53.19%	0.6348	0.184
		Average values for all data types	59.26%	58.49%	48.58%	0.73986	0.119
	Average values for Unsupervised learning methods		63%	66%	64%	0.69	0.11
Supervised learning methods	VGG16	OCT	81.06%	74.22%	93.06%	0.9485	0.121
		Segmented OCT	99%	100%	94.33%	0.9433	0.107
		FAF	98%	97.06%	98.98%	0.9901	0.115
		RCFP	53.76%	53.76%	53.77%	0.7515	0.147
		UWF	78%	78.72%	75.47%	0.8068	0.145
		Average values for all data types	81.96%	80.75%	0.83122	0.88804	0.127
	ResNet	OCT	72.5%	86.96%	69.47%	0.7345	0.144
		Segmented OCT	98.01%	100%	70.92%	0.7092	0.154

Preprints (www.preprints.org) | NOT PEER-REVIEWED | Posted: 21 November 2022 doi:10.20944/preprints202211.0392.v1

		FAF	96.50%	63.01%	85.18%	0.9066	0.164
		RCFP	50.25%	49.54%	52.63%	0.7653	0.132
		UWF	70.50%	66.95%	74.39%	0.8285	0.174
		Average values for all data types	77.55%	73.29%	0.70518	0.78882	0.1536
	Average values for Unsupervised learning methods		80%	77%	0.77	0.84	0.14
MLP-based fusion method for multiple data sources	The integrated database	OCT	94.06%	94.22%	93.26%	0.9607	0.074
		Segmented OCT	99%	98.41%	96.33%	0.9823	0.065
		FAF	90.11%	87.06%	88.98%	0.9401	0.096
		RCFP	93.76%	93.76%	93.77%	0.8924	0.121
		UWF	98.12%	97.06%	95.47%	0.9908	0.087
		The integrated database	97.4%	90.1%	86.24%	0.884	0.0886
	Average values for proposed method		95%	93%	0.92	0.94	0.09

4. Discussion

Data preprocessing for ophthalmologic images is a significant challenge, especially for images collected from multiple sources. It plays a vital role when it comes to enhancing the accuracy of eye disease diagnosis. Because of the wide angle of view, the UWF has been verified to have a great advantage for early screening of fundus disease. However, AI-based predicting model performing on the size of original figures exhibits a great challenge for engineering. An over compression process could make the important information missed (As the figure 12 shown). Thus, a ROI extraction is a necessary when it comes to UWF fundus disease detection. Besides, depsides of normal data enhancement of rotation, SPN adding, grey value processing and connected domain partition, GAN-based data generation approach presents a potential.

AMD is one of the most serious eye diseases leading to blindness. An early detection could lower the rate of visual rate. Since the short of ophthalmologists, especially in the developing areas, AI based methods exhibit a great strength. There are more than 7 images for AMD diagnosis. Because different images are with different features, a different preprocessing and enhancement method should be considered. This study verified that CGAN plays a good performance for OCT image enhancement. Segmented OCT generated by CFS segmentation on OCT database extract the lesion symptom of choroid and pre-macular membranes, which could be a potential method for AMD detection. However, important information could be missing. Picture binarization processes are performed on FAF images, CNV symptom is clearly detected in this image, which presents strengths for wet AMD diagnosis. However, fluorescence is asked to inject into the patient's eyes, which, which is a potential threat by causing the eye allergic action. The ROI extraction rule is verified effective by this study, which is defined as the area with the fovea as the center and the distance from the center of the optic disk (OD) to the fovea as the radius.

Under the comprehensively consideration, proposed fused source MLP-based method shows a great advantage for AMD detection with a low time-consuming and a high accuracy, sensitivity, specificity, and explainability. This method could be applied for each type of ophthalmologic images (OCT, segmented OCT, FAF, RCFP and UWF), which presents a practical contribution clinically. A reference value is delivered for other eye disease detection, especially for the ophthalmologic diagnosis based on multiple digital evidence, with complex diagnosis symptoms, or with low level of diagnosis diagnostic criteria. By comparing the average results values of accuracy, sensitivity, specificity, AUC and test time for all data types based on HC, SVM, ResNet-K Mean, VGG16, Res-Net and

 doi:10.20944/preprints202211.0392.v1

proposed method based on integrated database, SVM and ResNet is the most efficient method in unsupervised and supervised methods respectively. However, unsupervised learning model is unstable, it can't be guaranteed that specific number of clusters are outputted. Image based deep learning methods are resource consuming and low interpretability. Besides, comparing to the aforementioned digital ophthalmic image types, segmented OCT images present a distinct advantage for AMD diagnosis.

5. Conclusions

AI-based models present a great potential for AMD diagnosis. This study proposed a fused AI method based on multiple resources for AMD detection. Processes of image feature extractions, feature fusions and MLP-based predictions are involved. The characters and preprocess approaches of OCT, FAF, RCFP and UWF for AMD detection are discussed. Six methods for AMD diagnosis are experimented and compared. Findings show that the proposed method exhibits high performances for AMD detection, especially for colorful ophthalmic images. The most strength of this method is that it could detect AMD with one or more types of figures of the mentioned before. The real-world dataset of UWF from Shenzhen Aier hospital is involved for experiments. Clinical and theoretical contributions are delivered, reference value for other medical disease diagnosis based on digital images is indicated. It is recommended that more unsupervised and supervised models should be considered for the comparison. The explainable AI (EAI) mechanism should be discussed in the future. Labeled data enhancement methods based on Gan and EAI should be explored.

6. Patents

The Chinese patent named "The explainable AI method and system for AMD detection" (No. 2022104330486), "The classification method for AMD detection" (No. 2022104328005), "The explainable AI algorithm for AMD early screening" (No. 2022104329332) and "The algorithm of Macular fovea diagnosis" (202111329782. X) are related to this project.

Data Availability Statement: The UWF real-word dataset is an in-house dataset, which this article collected from Shenzhen Aier Eye Hospital. The "data access authorization & medical data ethics supporting document" from Shenzhen Aier Eye Hospital (both Chinese and English versions) of this study is available online at https://github.com/luckanny111/macular_fovea_detection.

Author Contributions: Conceptualization, Han Wang and Yi Pan; methodology, Han Wang and Junjie Zhou; software, Junjie Zhou, Zhoujie Tang and Chengde Huang; validation, Han Wang and Junjie Zhou; formal analysis, Han Wang and Junjie Zhou; investigation, Han Wang and Ruitao Xie; resources, Qinting Yuan and Lina Huang; writing—Han Wang; visualization, Han Wang and Junjie Zhou; supervision, Yi Pan and Kelvin KL Chong; funding acquisition, Han Wang. All authors have read and agreed to the published version of the manuscript.

Funding: This research was funded by 2020 Key Technology R&D Program of Guangdong Province under Grant 2020B1111540001, Zhuhai Technology and Research Foundation under Grant ZH22036201210034PWC, MOE (Ministry of Education in China) Project of Humanities and Social Science under Grant 22YJCZH213, The Science and Technology Research Program of Chongqing Municipal Education Commission under Grant KJZD-K202203601 and KJQN0202203605, KJQN202203607, and Natural Science Foundation of Chongqing China under Grant cstc2021jcyj-msxmX1108.

Informed Consent Statement: Informed consent was obtained from all subjects involved in the study.
Conflicts of Interest: The authors declare no conflict of interest.

Appendix A

The example of standardized fused feature matrix of image. Part of the matrix is illustrated as the following Table, the complete file is related to the supply material.

Table 2 The example of standardized fused feature matrix of image

Index of Image	Image types					Texture						Cluster labels			Image features extracted by ResNet
	OCT	Segmented OCT	FAF	RCFP	UWF	Image contrast	Dissimilarity	Homogeneit	Energy	Correlation	ASM	HC	SVM	ResNet-K Means	
1011_left.jpeg	0	0	1	0	0	1312.303346	19.88415404	0.1049168	0.01815471	0.85166455	0.00032959	3	0	2	1.1065844
1011_left.jpeg	0	0	1	0	0	1832.461147	23.51976457	0.10708811	0.01723316	0.79108936	0.00029698	0	0	0	0.43676913
1011_left.jpeg	0	0	1	0	0	1087.635197	18.21346457	0.12190159	0.01944228	0.87727262	0.000378	0	0	0	3.6655755
1011_left.jpeg	0	0	1	0	0	1781.264853	23.02067923	0.10791334	0.01739575	0.79692489	0.00030261	0	0	0	0.7981137
1011_left.jpeg	0	0	1	0	0	0	0	0	0	0	0	0	0	0	0
1011_left.jpeg	0	0	1	0	0	0	0	0	0	0	0	0	0	0	0.111185685
1011_left.jpeg	0	0	1	0	0	0	0	0	0	0	0	0	0	0	0
1011_left.jpeg	0	0	1	0	0	0	0	0	0	0	0	0	0	0	5.2078934
1011_left.jpeg	0	0	1	0	0	0	0	0	0	0	0	0	0	0	0.010217331
1011_left.jpeg	0	0	1	0	0	0	0	0	0	0	0	0	0	0	0.75168717
1011_left.jpeg	0	0	1	0	0	0	0	0	0	0	0	0	0	0	0.27491307

Preprints (www.preprints.org) | NOT PEER-REVIEWED | Posted: 21 November 2022 doi:10.20944/preprints202211.0392.v1

1011_left.jpeg	0	0	1	0	0	0	0	0	0	0	0	0	0	0	0
1011_left.jpeg	0	0	1	0	0	0	0	0	0	0	0	0	0	0	0
1011_left.jpeg	0	0	1	0	0	0	0	0	0	0	0	0	0	0	0.6293562
1011_left.jpeg	0	0	1	0	0	0	0	0	0	0	0	0	0	0	0
1011_left.jpeg	0	0	1	0	0	0	0	0	0	0	0	0	0	0	0.07629201
1011_left.jpeg	0	0	1	0	0	0	0	0	0	0	0	0	0	0	0
1011_left.jpeg	0	0	1	0	0	0	0	0	0	0	0	0	0	0	0.6372398
1011_left.jpeg	0	0	1	0	0	0	0	0	0	0	0	0	0	0	0.67938274

References

1. Wang H. A Bibliographic Study and Quantitative Analysis of Age-related Macular Degeneration and Fundus Images. Annals of Ophthalmology and Visual Sciences 2022;5:1-8.
2. KURT RA, MESTANOGLU M. Ultra-widefield Imaing in Age-Related Macular Degeneration. Retina-Vitreus/Journal of Retina-Vitreous 2021;30.
3. Yang J, Fong S, Wang H, Hu Q, Lin C, Huang S, Shi J, Lan K, Tang R, Wu Y. Artificial intelligence in ophthalmopathy and ultra-wide field image: A survey. Expert Systems with Applications 2021;182:115068.
4. Wang H. A Survey of AI to AMD and Quantitative Analysis of AMD Pathology Based on Medical Images. Artificial Intelligence and Robotics Research 2022;11:143-57.
5. Grassmann F, Mengelkamp J, Brandl C, Harsch S, Zimmermann ME, Linkohr B, Peters A, Heid IM, Palm C, Weber BH. A deep learning algorithm for prediction of age-related eye disease study severity scale for age-related macular degeneration from color fundus photography. Ophthalmology 2018;125:1410-20.
6. Alone A, Chandra K, Chhablani J. Wide-field imaging-An update. Indian Journal of Ophthalmology 2021;69:788.
7. Schmitz-Valckenberg S, Holz FG, Bird AC, Spaide RF. Fundus autofluorescence imaging: review and perspectives. Retina 2008;28:385-409.
8. Huang NT, Georgiadis C, Gomez J, Tang PH, Drayna P, Koozekanani DD, van Kuijk FJ, Montezuma SR. Comparing fundus autofluorescence and infrared imaging findings of peripheral retinoschisis, schisis detachment, and retinal detachment. American journal of ophthalmology case reports 2020;18:100666.
9. Treder M, Lauermann JL, Eter N. Automated detection of exudative age-related macular degeneration in spectral domain optical coherence tomography using deep learning. Graefe's Archive for Clinical Experimental Ophthalmology 2018;256:259-65.
10. Spaide RF, Fujimoto JG, Waheed NK, Sadda SR, Staurenghi G. Optical coherence tomography angiography. Progress in retinal eye research 2018;64:1-55.
11. DuBose TB, LaRocca F, Farsiu S, Izatt JA. Super-resolution retinal imaging using optically reassigned scanning laser ophthalmoscopy. Nature photonics 2019;13:257-62.
12. Hirano T, Imai A, Kasamatsu H, Kakihara S, Toriyama Y, Murata T. Assessment of diabetic retinopathy using two ultra-wide-field fundus imaging systems, the Clarus® and Optos™ systems. BMC ophthalmology 2018;18:1-7.
13. Chua PY, Sandinha MT, Steel DH. Idiopathic epiretinal membrane: progression and timing of surgery. Eye 2022;36:495-503.
14. Chen C, Sharma S, Mammo D, Baynes K, Ehlers JP, Srivastava SK. Identification of Retinal Fluid Accumulation in Uveitis Patients with Normal Foveal Contour on OCT and Retinal Vascular Leakage on Ultra-Widefield Fluorescein Angiography. Investigative Ophthalmology Visual Science 2022;63:4459–F0138-4459–F0138.
15. Touhami S, Béguier F, Yang T, Augustin S, Roubeix C, Blond F, Conart JB, Sahel JA, Bodaghi B, Delarasse C. Hypoxia Inhibits Subretinal Inflammation Resolution Thrombospondin-1 Dependently. International Journal of Molecular Sciences 2022;23:681.
16. Ehlers JP, Patel N, Kaiser PK, Heier JS, Brown DM, Meng X, Reese J, Lunasco L, Le TK, Hu M. The Association of Fluid Volatility With Subretinal Hyperreflective Material and Ellipsoid Zone Integrity in Neovascular AMD. Investigative ophthalmology visual science 2022;63:17-.
17. Deng Y, Qiao L, Du M, Qu C, Wan L, Li J, Huang L. Age-related macular degeneration: Epidemiology, genetics, pathophysiology, diagnosis, and targeted therapy. Genes diseases 2022;9:62-79.
18. Vander JF, Borne MJ. Retinal detachment. Ophthalmology Secrets E-Book 2022:366.
19. Zhang L, Jing'an T. The Experience of Professor Tong Jing'an in Treating Age Related Macular Disease. MEDS Public Health Preventive Medicine 2022;2:71-4.
20. Damian I, Nicoară SD. SD-OCT Biomarkers and the Current Status of Artificial Intelligence in Predicting Progression from Intermediate to Advanced AMD. Life 2022;12:454.

 doi:10.20944/preprints202211.0392.v1

21. Bou Ghanem G, Neri P, Dolz-Marco R, Albini T, Fawzi A. Review for Diagnostics of the Year: Inflammatory Choroidal Neovascularization–Imaging Update. Ocular Immunology Inflammation 2022:1-7.

22. Yeo NJY, Chan EJJ, Cheung C. Choroidal neovascularization: Mechanisms of endothelial dysfunction. Frontiers in Pharmacology 2019;10:1363.

23. Zaman N, Ong J, Tavakkoli A, Zuckerbrod S, Webster M. Adaptation to Prominent Monocular Metamorphopsia using Binocular Suppression. Journal of Vision 2022;22:11-.

24. Bourauel L, Vaisband M, von der Emde LA, Bermond K, Tarau IS, Sassmannshausen M, Heintzmann R, Holz FG, Curcio CA, Hasenauer J. Spectral analysis of human retinal pigment epithelium cells in healthy and AMD affected eyes. Investigative Ophthalmology Visual Science 2022;63:4621–F0413-4621–F0413.

25. Douglas VP, Garg I, Douglas KA, Miller JB. Subthreshold Exudative Choroidal Neovascularization (CNV): Presentation of This Uncommon Subtype and Other CNVs in Age-Related Macular Degeneration (AMD). Journal of Clinical Medicine 2022;11:2083.

26. Notomi S, Shiose S, Fukuda Y, Mori K, Hashimoto S, Kano K, Ishikawa K, Sonoda K-H. Characteristics of retinal pigment epithelium elevations preceding exudative age-related macular degeneration in Japanese. Ophthalmic Research 2022.

27. Beltramo E, Mazzeo A, Porta M, editors. Extracellular Vesicles Derived from M1-Activated Microglia Induce Pro-Retinopathic Functional Changes in Microvascular Cells. 32nd Meeting of the European Association for Diabetic Eye Complications (EAsDEC); 2022.

28. Jidigam VK, Singh R, Batoki JC, Milliner C, Sawant OB, Bonilha VL, Rao S. Histopathological assessments reveal retinal vascular changes, inflammation, and gliosis in patients with lethal COVID-19. Graefe's Archive for Clinical Experimental Ophthalmology 2022;260:1275-88.

29. Conedera FM, Enzmann V. Regenerative capacity of Müller cells and their modulation as a tool to treat retinal degenerations. Neural Regeneration Research 2023;18:139.

30. Damato BE. Anterior Intraocular Lesions. Clinical Atlas of Ocular Oncology. Springer; 2022. p. 79-136.

31. Wang H, Li Z. The application of machine learning and deep learning to Ophthalmology: A bibliometric study (2000-2021). In: Tareq A, Taiar R, editors. Human Interaction & Emerging Technologies (IHIET-AI 2022): Artificial Intelligence & Future Applications. 2022.

32. Han W. A Review of Artificial Intelligence in Ophthalmology Field—Taking the Fundus Diagnosis Based on OCT Images as an Example. Artificial Intelligence and Robotics Research 2021;10:306-12.

33. Wang H, Hou G, Wu Y, Pan Y, Xing L, Yang J, Chong KK-l, Du W, Fong S, Duan Y, Yao X, Zhou X, Li Q, Wu F, Chen L, Liu J, Lina H. Deep learning for macular fovea detection based on ultra-widefield Fundus images. Computational and Mathematical Methods in Medicine 2022.

34. Singh A, Pandey B. A new intelligent medical decision support system based on enhanced hierarchical clustering and random decision forest for the classification of alcoholic liver damage, primary hepatoma, liver cirrhosis, and cholelithiasis. Journal of healthcare engineering 2018;2018.

35. Gogineni S, Pimpalshende A, Goddumarri S. Eye Disease Detection Using YOLO and Ensembled GoogleNet. Evolutionary Computing and Mobile Sustainable Networks. Springer; 2021. p. 465-82.

36. Al-Zoubi AM, Heidari AA, Habib M, Faris H, Aljarah I, Hassonah MA. Salp chain-based optimization of support vector machines and feature weighting for medical diagnostic information systems. Evolutionary machine learning techniques. Springer; 2020. p. 11-34.

37. Chhabra M, Kumar R. An Advanced VGG16 Architecture-Based Deep Learning Model to Detect Pneumonia from Medical Images. Emergent Converging Technologies and Biomedical Systems. Springer; 2022. p. 457-71.

38. Ikechukwu AV, Murali S, Deepu R, Shivamurthy R. ResNet-50 vs VGG-19 vs training from scratch: a comparative analysis of the segmentation and classification of Pneumonia from chest X-ray images. Global Transitions Proceedings 2021;2:375-81.

 doi:10.20944/preprints202211.0392.v1

39. Lorencin I, Anđelić N, Španjol J, Car Z. Using multi-layer perceptron with Laplacian edge detector for bladder cancer diagnosis. Artificial Intelligence in Medicine 2020;102:101746.
40. Retinal OCT Images (optical coherence tomography) [database on the Internet]. Kaggle. 2018. Available from: https://www.kaggle.com/datasets/paultimothymooney/kermany2018. Accessed:
41. Retinal OCT - C8 [database on the Internet]. Kaggle. 2021. Available from: https://www.kaggle.com/datasets/obulisainaren/retinal-oct-c8. Accessed:
42. Retinal Fundus Images [database on the Internet]. Kaggle. 2021. Available from: https://www.kaggle.com/datasets/kssanjaynithish03/retinal-fundus-images. Accessed:
43. Retinal Disease Classification [database on the Internet]. Kaggle. 2021. Available from: https://www.kaggle.com/datasets/andrewmvd/retinal-disease-classification. Accessed:
44. Ocular Disease Recognition [database on the Internet]. Kaggle. 2020. Available from: https://www.kaggle.com/andrewmvd/ocular-disease-recognition-odir5k. Accessed:
45. Liang Z, Huang JX, Li J, Chan S, editors. Enhancing automated COVID-19 chest X-ray diagnosis by image-to-image GAN translation. 2020 IEEE International Conference on Bioinformatics and Biomedicine (BIBM); 2020: IEEE.
46. Mirza M, Osindero S. Conditional generative adversarial nets. arXiv preprint arXiv:14111784 2014.
47. Mousavi SM, Naghsh A, Manaf AA, Abu-Bakar S. A robust medical image watermarking against salt and pepper noise for brain MRI images. Multimedia Tools Applications 2017;76:10313-42.
48. Dong B, Li H, Sun J, Mari GM, Yu X, Ke Y, Li J, Wang Z, Yu W, Wen K. Development of a fluorescence immunoassay for highly sensitive detection of amantadine using the nanoassembly of carbon dots and MnO2 nanosheets as the signal probe. Sensors Actuators B: Chemical 2019;286:214-21.
49. Karegowda AG, Jayaram M, editors. Cascading GA & CFS for feature subset selection in medical data mining. 2009 IEEE International Advance Computing Conference; 2009: IEEE.
50. Ozcift A, Gulten A. Classifier ensemble construction with rotation forest to improve medical diagnosis performance of machine learning algorithms. Computer methods programs in biomedicine 2011;104:443-51.
1.